Published in final edited form as:
Stem Cells. 2009 September ; 27(9): 2362–2370. doi:10.1002/stem.163.

Neural stem cell transplantation benefits a monogenic neurometabolic disorder during the symptomatic phase of disease

Mylvaganam Jeyakumar[a,*], **Jean-Pyo Lee**[b,c,*], **Nicola R Sibson**[d], **John P Lowe**[d], **Daniel J Stuckey**[d], **Katie Tester**[a], **Gerald Fu**[b], **Robbin M Newlin**[b], **David A Smith**[a], **Evan Y Snyder**[b,c,¶], and **Frances M Platt**[a,¶]

[a]Department of Pharmacology, University of Oxford, Mansfield Road, Oxford 0X1 3QT, UK

[b]Stem Cell & Regeneration Program, Center for Neuroscience and Aging Research, Burnham Institute for Medical Research, La Jolla, California 92037, USA

[c]Department of Pediatrics, University of California, San Diego, School of Medicine, La Jolla, California 92093, USA

[d]Experimental Neuroimaging Group, Department of Physiology, Anatomy and Genetics University of Oxford, Parks Road, Oxford, OX1 3PT, UK

Abstract

Although we and others have demonstrated that neural stem cells (NSCs) may impact such neurogenetic conditions as lysosomal storage diseases when transplanted at birth, it has remained unclear whether such interventions can impact well-established mid-stage disease, a situation often encountered clinically. Here we report that when NSCs were injected intracranially into the brain of adult symptomatic Sandhoff (*Hexb*$^{-/-}$) mice, cells migrated far from the injection site and integrated into the host cytoarchitecture, restoring β-hexosaminidase enzyme activity and promoting neuropathologic and behavioral improvement. Mouse lifespan increased, neurological function improved, and disease progression was slowed. These clinical benefits correlated with neuropathological correction at the cellular and molecular levels, reflecting the multiple potential beneficial actions of stem cells, including enzyme cross-correction, cell replacement, tropic support, and direct anti-inflammatory action. Pathotropism, i.e., migration and homing of NSCs to pathological sites, could be imaged in real time by magnetic resonance imaging. Differentially expressed chemokines might play a role in directing the migration of transplanted stem cells to sites of pathology. Because many of the beneficial actions of NSCs observed in newborn brains were recapitulated in adult brains to the benefit of Sandhoff recipients, NSC-based interventions may also be useful in symptomatic subjects with established disease, even in symptomatic patients.

¶To either of whom correspondence may be sent: EYS (esnyder@burnham.org) or FMP (frances.platt@pharm.ox.ac.uk).
*JPL and MJ contributed equally to this study

Author Contributions:
M.J and J-P.L: Conception and design, collection and/or assembly of data, data analysis and interpretation, manuscript writing.
N.R.S, and D.J.S: MRI data collection, analysis and interpretation.
K.T, G.F, R.M.N: Collection and/or assembly of data.
D.A.S: Collection and/or assembly of data for neurological function and survival.
E.Y.S and F.M.P: Overall conception and design, provision of study material, data analysis and interpretation, financial support, manuscript writing, final approval of manuscript.

Keywords

neural stem cell therapy; lysosomal storage disorders; Sandhoff disease; neurodegenerative disease; metabolic cross-correction

INTRODUCTION

Understanding and optimising cellular reparative mechanisms is fundamental to stem cell therapy for brain repair. Among neurodegenerative conditions, Sandhoff disease is one of a group of metabolic disorders termed lysosomal storage disorders (LSDs) (1). Documented abnormalities in LSDs include inflammation, oxidative stress, and apoptotic neuronal death (2–4). Although no effective therapies currently exist for LSDs with central nervous system (CNS) involvement and most other neurodegenerative disorders, stem cells may offer therapeutic options, by invoking multiple beneficial mechanisms.

Sandhoff disease results from the autosomal recessive inheritance of mutations in the β-subunit of β-hexosaminidase (Hex) gene resulting in accumulation of the undegraded glycosphingolipids (GSLs) GM2 and GA2 within lysosomes of cells of the central nervous system. Sandhoff (*Hexb*$^{-/-}$) mice, generated by targeted disruption of *Hexb* encoding the β-subunit of hexosaminidase A(αβ) and B(ββ), develop a fatal neurodegenerative disease, which prevents survival beyond about 4 months (5,6). *Hexb*$^{-/-}$ mice mimic clinical features of human Tay-Sachs and Sandhoff diseases. Sandhoff disease also shares several convergent pathological and phenotypic features with Alzheimer and Parkinson diseases (7), such as CNS inflammation, secondary α-synuclein pathologies (8), and altered calcium homeostasis and endosomal/lysosomal function (7,9).

Neural stem cells (NSCs) promote donor-to-recipient cross correction via enzyme secretion-recapture, but can also mediate cell replacement, cell rescue through tropic support, growth factor secretion, neurogenic or gliogenic regulator secretion, and/or other mechanisms such as anti-inflammatory or immune modulatory effects (10–12). We previously demonstrated its clinical benefits when administered at postnatal day 1 in the Sandhoff disease mouse model (12). However, the major clinical challenge is to develop therapies that are effective in symptomatic individuals, as patients generally exhibit symptoms at the time of diagnosis (13). As such, in this study, as proof-of-concept we treated adult symptomatic Sandhoff disease mice with a single injection of unengineered murine NSC lines into the hippocampus. The hippocampus was chosen because of its pivotal role in cognition, yet represented on index point from which wider migration could be assayed.

MATERIALS AND METHODS

Mice

The generation of Sandhoff (*Hexb*$^{-/-}$) mice has been described (5,6). Mice were genotyped by the polymerase chain reaction (PCR) from tail DNA (5,6). All mice were bred and housed under nonsterile conditions, with food and water available *ad libitum*. All animal studies were conducted using protocols approved by the UK Home Office Licence (Animal Scientific Procedures Act, 1986). Animals used in the experiments were 12 to 13 weeks old (midsymptomatic).

NSC culture and transplantation

Cloned NSCs from well-described and well-characterized NSC line, C17.2, was maintained as previously described (14–18). Briefly, the cells, which constitutively express lacZ, were grown in Dulbecco's modified Eagle's medium (DMEM) supplemented with 10% fetal calf

serum, 5% horse serum, 2 mM glutamine, penicillin (100 μ/ml) and streptomycin (100 mg/ml), on uncoated 10 cm tissue culture dishes. Near-confluent cells were trypsinized, washed three times with PBS and resuspended in PBS at a final concentration of 80,000 cells/μl.

For stereotactic injection, mice were anesthetised with isofluorane integrated in the KOPF® stereotaxic frame, their eyes applied with occular ointment to prevent drying, their heads wiped clean with 70% ethanol, and their skin cut opened at midline. A small cranial burr hole (0.9 mm diameter) was made on a premarked skull area (2 mm posterior to bregma; 1.5 mm lateral to sagittal suture) with a dental drill bit. Using a pulled-glass micropipette, 4 μl containing ~320,000 viable cells was injected over a 4-minute period into the brain through the hole in the skull (depth; 2 to 2.5 mm dorsal). The wound was closed with cyanoacrylate glue (Vectabond). Mock grafted controls received the same volume of PBS.

The experimental groups of adult mice used were as follows: Sandhoff NSC treated (n=28), Sandhoff Sham treated (n=24), Wild type NSC treated (n=20), and Wild type Sham treated (n=20). For biochemical and histological evaluation, some animals were killed before their natural end-points where indicated.

Neurological function and survival

Mice were tested individually, randomizing subjects with respect to treatment, test sequence, and sex. The outcome was evaluated using behavioral tests previously validated for this model (19–22). A horizontal bar-crossing test (n=7–12 animals per group) was used to appraise motor coordination and hind-limb strength as described previously (20). A humane endpoint was applied when the mice became moribund and were no longer able to right themselves within 20 seconds of being laid on their side.

For the open field test (n=6 animals per group), spontaneous motor and posture patterns (locomotion and rearing frequency) were recorded for each animal during a 3 minute test period in an automated activity monitor AM1053 (Linton Instruments). The instrument uses an array of infrared beams to determine activity and mobility of a subject. The AmLogger software in this instrument automatically logs the number of infrared beam breaks in the X–Y plane (locomotion) and vertical plane (rearing) in a given period of time that the animals spend in the monitoring cage.

Tissue processing

Recipient mice were sacrificed by CO_2 asphyxiation and immediately perfused with 50 ml of heparinized saline, followed by 100 ml of 4% paraformaldehyde (PFA) fixative (PBS containing 4% PFA, 2-mM $MgCl_2$ and 1.25-mM EGTA, pH 7.4). Brains were removed, postfixed for 4–6 hours at 4°C, cryoprotected in 30% sucrose solution at 4°C overnight, and freeze-embedded in OCT (BDH) for sectioning. Coronal sections (10 μm) were collected every one in ten intervals, placed onto glass microscope slides, air dried for 4–6 hours, and stored at −70°C prior to histological examination. Unfixed PBS-perfused brains were processed for biochemical analysis where indicated.

Detecting NSC engraftment

Serial coronal sections of recipient brains were processed for lacZ expression by NSCs using X-gal histochemistry or anti β-gal immunohistochemistry, as described previously (11,15).

X-gal histochemistry—Fixed cryostat sections were rehydrated in rinse solution (PBS containing 2 mM $MgCl_2$ and 1.25 mM EGTA, pH 7.4), permeabilized in detergent (PBS containing 2 mM $MgCl_2$, 1.25 mM EGTA and 0.02% Nonidet P-40, pH 7.4) and incubated in freshly prepared X-gal buffer containing 1 mg/ml of 5-bromo-4-chloro-3-indolyl-β-D-

galactosidase) (X-gal, Promega), 2 mM $MgCl_2$, 5 mM $K_4Fe(CN)_6$, 5 mM $K_3Fe(CN)_6$ in PBS at pH 8.3. Following incubation at 37 °C overnight, cells were counterstained with nuclear red.

Immunohistochemistry—β-gal was detected with a mouse monoclonal antibody (mAb) (Promega) or a rabbit polyclonal antibody (pAb) (ICN/Cappel). Cell type-specific antigens were detected with the following antibodies: Pan-neuronal neurofilament marker (pan-NF) with mouse mAb (Sternberger); NeuN with a mouse mAb (Chemicon); glial fibrillary acidic protein (GFAP) with a rabbit pAb (Sigma); myelin basic protein (MBP) with a rabbit pAb (Sigma). Primary antibodies were detected with secondary antibodies coupled to fluorochromes Alexa Fluor 488 or FITC and Alexa Fluor 594 or Texas Red.

The composition of neural cell types from engrafted donor-derived cells was calculated by counting the total number of $\beta\text{-gal}^+$ cells (donor cell marker) in matched coronal brain sections (n=3), in combination with differentiation-specific markers (NeuN or NF for neurons, GFAP for astroglia, and MBP for oligodendrocytes) or Nestin (undifferentiated NSC marker) used in fluorescence light microscopy (Axiostar Plus, Carl Zeiss).

Confocal microscopy—Images were acquired using a Bio-Rad MRC 1024 equipped with a single photon Kr/Ar laser and a Bio-Rad Radiance 2100MP equipped with a multiphoton laser and taken at 1024 × 1024 pixel resolution. Images were acquired sequentially to negate channel cross-talk. Negative and positive control images were taken with the same settings. Each merged image was visualized using orthogonal projections composed of 9–16 optical Z-planes 0.5- to 1-μm thick.

In vivo magnetic resonance imaging (MRI)

NSCs were labeled with the MRI contrast agent Sinerem® (ultra-small super-paramagnetic iron-oxide particles, gift of C. Corot, Guerbet, France), introduced into the cells by lipofection using the reagent FuGENE according to the manufacturer's instructions (23). MRI data were acquired using a 9.4 Tesla vertical bore magnet with a Varian Inova spectrometer (Varian, Palo Alto, CA). MRI was performed on both Sandhoff and wild-type control mice 24 hours after transplantation with ~320,000 viable stem cells, then repeated at 2, 3, and 5 weeks postinjection (n=2 per group). Animals were positioned in an Alderman-Grant resonator using a bite bar to prevent movement of the head during image acquisition. Coronal slices centered at the level of the injection site were selected for the imaging protocol. Spin-echo T1-weighted images (TR=0.5 sec, TE=20 msec) and fast spin-echo T2-weighted images (TR=3.0 sec, TE=40 msec, 5 echoes) were acquired in the coronal plane (1 mm slice; FOV=3 cm × 3 cm, 128 × 128 matrix). During MRI data collection, anesthesia was maintained with 0.5%–1.2% isoflurane in 70% N_2O:30% O_2. ECG was monitored, and body temperature was maintained at ~37°C.

GSL storage analysis

For *in situ* detection of GSL storage, brain sections were processed using the periodic acid/Schiff reagent (PAS) as described previously (20). Quantitative analysis of GSLs was according to fluorescence detection of GSL-derived oligosaccharides by high-performance liquid chromatography (HPLC) as previously described (24), with slight modifications. Briefly, comparable areas (4 mm^2) of brain regions were scraped from slides into a screw-capped Eppendorf tube, sonicated in 50 μl of distilled water, extracted with 200 μl of chloroform-methanol (2:1, v/v) for 3 hours at room temperature, and spun in a microfuge (13,000 rpm) for 5 minutes after which the supernatants were transferred and dried under a stream of nitrogen prior to ceramide glycanase digestion as described (24). The released oligosaccharides were fluorescently labeled with anthranilic acid, purified through

Discovery DPA-6S columns (Sigma), and separated via normal-phase HPLC with fluorescence detection. In addition to HPLC, thin-layer chromatography (TLC) quantification was also used to analyze GM2 and GA2 storage on the brain slices (20).

β-hexosaminidase determination

For quantitative enzyme assays, comparable cortical tissues were homogenized in 0.5 ml of H_2O using an Ultraturax T25 probe, spun in a microfuge (13,000 rpm) for 20 seconds. The supernatant retained for assay. Hex activity of the sample was determined by incubating 10 μl of the supernatant enzyme source with 50 μl of 3 mM 4-MUGlcNAc in 100 mM citrate/ 200 mM sodium phosphate buffer, pH 4.5, for 30 minutes at 37°C. The reaction was stopped with 200 ml of NaOH-Glycine (0.3 M, pH 10.5), and the released 4-MU was measured at 365/460 nm ex/em (Perkin Elmer fluorimeter). Activity was standardized to protein concentration (Bio-Rad protein assay).

RT-PCR

Gene expression was analyzed by reverse transcriptase-PCR (RT-PCR). Total RNA was extracted from tissue samples using an RNeasy Protect Mini Kit (QIAGEN) according to the manufacturer's instructions. RNA was reverse transcribed into cDNA with Quantiscript Reverse Transcriptase using a QuantiTect® Kit (QIAGEN). Quantification of different mRNAs was performed by PCR on a PTC-200 DNA Engine thermal cycler (MJ Research).

PCR amplification was performed with 1 μl of reverse transcriptase reaction mixture in 45 μl of Platinum PCR® SuperMix (Invitrogen) containing 22 mM Tris-HCl (pH 8.4), 55-mM KCl, 1.65 mM MgCl2, 0.22 mM of each dNTP, 0.2 μM per primer (listed below), and 1 unit of recombinant Taq DNA polymerase with Platinum Taq antibody. PCR conditions were as follows: denaturation at 94°C for 20 seconds, primer annealing at 60°C (TNFα, IL1β, IL6) or 59°C (Mac1α, MIP1α) or 58°C (iNOS, SCF, c-Kit) or 54°C (F4/80, 18S rRNA) or 46°C (Hexb β subunit) for 20–45 seconds; and primer extension was incubated at 72°C for 60 seconds. Cycle numbers were adjusted to keep the PCR amplification in log phase for semi-quantitation (23 to 29 cycles depending on the amount of template cDNA used).

Following PCR, the amplified products (332 bp for TNFα; 341 bp for IL1β; 328 bp for MIP1α; 340 bp for IL6, iNOS, SCF, and cKit; 118 bp for Hexb β subunit; and 137 bp for 18s rRNA) were stained with ethidium bromide on a 3% agarose gel and visualized. The band intensities were quantified and values normalized to 18S rRNA levels.

Statistics

Survival data were analysed using the Log-rank test (n=10–12 per group). Motor-function decline (horizontal bar-crossing test) was assessed using repeated-measures analysis of variance (ANOVA) (n=7–12 per group). An unpaired two-tailed Student's t-test was used to analyze the following data: locomotion and rearing activity (open-filed test, n=6 per group), RT-PCR of inflammatory and/or chemotactic markers (n=3–5 per group), quantitative Hex assays (n=3 per group), and quantitative GSL storage analysis (n=3–5 per group).

RESULTS

NSCs engraft robustly in symptomatic Sandhoff disease mice

LacZ-expressing neural stem cells were transplanted into the hippocampus of one hemisphere at 12–13 weeks of age (Fig. 1, I). This is the midsymptomatic phase of the disease when mice have already developed extensive CNS inflammation involving not only microglial activation but also peripheral monocyte recruitment to the brain(2–4). Mice also exhibit tremor, mild ataxia, and muscle weakness, surviving only an additional 4 weeks.

Donor NSCs were detected in diverse brain regions, ranging from the injection site to the noninjected contralateral hemisphere 2 weeks posttransplantation (n=7, Fig. 1, I A–C shows representative image), and the engraftment was stable for the life of the mouse (Fig. 1II A B). A typical coronal section through the injection site revealed engraftment in most cortical areas of the injected hemisphere, with migration to the contralateral cortex (Fig. 1, IA), including to the contralateral hippocampus (Fig. 1, I B). In transplanted wild type brains, such widespread cell migration did not occur as determined X-gal histochemcial staining. Instead, most transplanted cells remained at the injection site (data not shown).

MRI imaging permitted engraftment to be monitored in Sandhoff disease mice longitudinally and noninvasively in real time up until sacrifice (at least 5–6 weeks posttransplant) (Fig. 1, II). Migration of iron-laden stem cells along the medial margin of the hippocampus was clearly detected as an area of signal void (Black). (Fig. 1, II). Increased cell accumulation was evident up to day 38 posttransplantation (Fig. 1, II). Even in symptomatic, end-stage Sandhoff mice, NSCs (Black) migrate from their point of implantation (red arrow) to regions of pathology, likely represented by T2 hyperintensity (white, yellow arrow), in a manner not seen in transplanted wild type mice. It is this diffuse spread of NSCs from their point of injection that likely contributed to the functional improvements noted below.

Transplants delay disease progression and increase lifespan

Mice transplanted in the right hippocampus alone had an increased life expectancy relative to untreated SD controls (19%, $p<0.0001$, Log-rank test, n=10–12 per group) (Fig. 2B). At 15-weeks old, treated SD mice had improved neurological function relative to sham-transplanted SD mice, as evidenced by locomotion and rearing activity (Fig. 2C–D, n=6 per group). Locomotion values in the treated SD mice were at 75% of wild-type levels, as opposed to the 50% of wild-type levels exhibited by sham-transplanted SD controls, yielding approximately 25% functional protection ($p=0.006$) (Fig. 2C). Rearing activity declined rapidly in the untreated SD controls, reaching 5% of normal by 15 weeks of age with a loss of 95% function. However, this decline was prevented in part in NSC-treated SD mice, which lost only 50% of wild-type rearing activity overall, yielding approximately 45% functional protection ($p=0.013$) (Fig. 2D).

In the horizontal bar-crossing test to evaluate changes in motor coordination and muscle strength (Fig. 2E), sham-treated SD mice showed a rapid decline in motor function until 15 weeks of age and then reached a plateau. By contrast, functional decline was partially prevented after NSC treatment, an improvement that continued for about 4 weeks, when a plateau was reached towards the terminal stage. Repeated two-way ANOVA analysis demonstrated a significant effect for NSC versus sham controls in motor function ($p< 0.0001$) (Fig. 2E, n=7–12 per group)

NSC engraftment decreases lysosomal storage levels

NSC-treated SD mice showed a marked reduction of GSL storage in the brain relative to untreated SD controls, as evidenced by PAS-staining. Such a decrease was seen in both injected and noninjected hemispheres (Fig. 3) and positively correlated with X-gal staining (Fig. 1, I), a marker for NSC distribution. Thus, the NSCs had migrated to the side contralateral to the injection. Greater clearance of GSL storage was observed in the injected versus noninjected hemisphere (e.g., hippocampus CA3 region and mediodorsal thalamic nucleus, Fig. 3B, C, and F). Nevertheless, PAS staining of the noninjected hemisphere of the treated SD mice bore decreased GSL storage compared to control sham-injected brains (e.g., hippocampus CA3 region, Fig. 3A and C). Donor-derived enzyme did clear GSL storage in host cells at distances even far from the single injection site.

To quantify changes in lysosomal storage levels, lipids were extracted from microdissected brain regions and analyzed by a highly sensitive HPLC assay (24). At 2 weeks posttransplant (15 weeks of age), a representative HPLC profile of a microdissected cortical lipid extraction is shown in fig 4G. Compared to levels in the sham-treated controls, GM2 was reduced by 19±1% ($p=0.004$), and GA2 was reduced by 8±0.3% ($p=0.015$) in the treated mice (Fig. 3G).

To determine the extent of metabolic cross-correction, brain hemispheres from transplanted and control mice were extracted, and lipids were analyzed from serial coronal brain slices taken at various distances from the injection site, using standard HPTLC (Supplementary Fig. 1). Interestingly, at 4 weeks posttransplant, GM2 reduction was seen as far away as 4 mm (posterior) from the graft site, with a more significant reduction occurring closer to the graft site. For GA2, this reduction occurred as far as 6-mm posterior to the graft site. Notably, reductions were seen in both the ipsilateral-injected and contralateral-uninjected sides, although, as expected, greater GM2 reduction (45%, $p=0.008$) was seen in the ipsilateral area compared to the contralateral (24%, $p=0.007$) hemisphere (Supplementary Fig. 1).

Transplanted mice show reconstituted Hex activity

To determine the extent of Hex reconstitution, we measured enzyme activity (Fig 4). Quantitative Hex assays of homogenates of sections taken from X-gal$^+$ brain areas revealed a significant increase in Hex activity (up to 6% of wild-type levels, $p<0.001$) compared with age-matched SD controls that did not receive transplants (Fig. 4A). It bears noting that as little as 2–5% of normal levels can restore normal metabolism to mutant cells. We followed enzyme distribution by assaying Hex activity in serial slices of coronal brain sections. Activity was restored both in injected and noninjected contralateral hemispheres, which exhibited 1%–6% and 1%–3% of wild-type levels, respectively (Fig. 4A). Accordingly, spatial distribution of enzyme activity was inversely correlated with GSL storage (Supplementary Fig. 1). *In situ* histochemistry of Hex activity in coronal brain sections of NSC-treated SD mice showed positive staining in various brain areas, indicative of graft survival and widespread migration (data not shown). Spatial distribution of enzyme activity coincided with X-gal$^+$ areas and was inversely correlated with GSL storage levels.

To gain further insights into stem cell migration and engraftment and verify Hex activity, we isolated total RNA from four distinct brain regions of individual hemispheres (dorsal cortex, thalamus, lateral cortex, and hippocampus) and analyzed β-subunit expression of Hex using conventional RT-PCR (Fig. 4B). In the treated mice, β-subunit expression was detected in multiple brain regions, including the hippocampus and dorsal cortex and in both hemispheres, in agreement with the X-gal and Hex assays (Fig. 4B).

Effects of NSCs on CNS inflammation

CNS inflammation characterized by microglial activation is a hallmark of lysosomal storage diseases (2–4). We, therefore, examined the impact of NSC therapy on inflammation in Sandhoff mice using RT-PCR of inflammatory and/or chemotactic markers in the brain (Fig. 5). Elevated expression of the proinflammatory cytokines TNFα and IL-1β was observed in the Sandhoff mouse brain compared to wild-type mice. The activated microglial/macrophage marker Mac1α (Cd11b) was upregulated ~8-fold in the Sandhoff mouse brain relative to the wild type, while no significant variation was seen in IL-6, iNOS, SCF or c-kit (Fig. 5B). More importantly, the chemokine MIP1α (also known as CCL3) was highly upregulated in the Sandhoff brain (6-fold increase, $p<0.001$). All these upregulated genes are indicators of macrophage/microglial activation or the response of reactive astrocytes and neurons (25) to lysosomal pathology. NSC treatment decreased expression of inflammatory

genes such as TNFα, IL-1β, Mac1α, and MIP1α compared to untreated SD controls. Similar effects were seen in the contralateral hemisphere (data not shown).

NSC differentiation phenotypes

Differentiation of transplanted NSCs was assessed by immunocytochemistry using lineage-specific markers, namely, "pan"-neurofilaments (NF) for neurons, glial fibrilliray acidic protein (GFAP) for astroglia, myelin basic protein (MBP) for oligodendrocytes and nestin for undifferentiated NSCs. Two to 3 weeks posttransplantation, microscopic analysis of immunostained sections revealed that a subset of transplanted cells differentiated into multiple cell types, including neurons (Fig. 6 and Supplementary Fig. 2). Migratory β-gal$^+$ cells in the hippocampal CA2/CA3 region and the thalamus MCLH (magnocellular nucleus of lateral hypothalamus) region differentiated into neurons, as evidenced by pan-NF expression (Supplementary Fig. 2). Donor-derived astrocytes were also detected (in cortical and hippocampal areas), as revealed by GFAP-β-gal double labeling and morphological identity (Fig. 6C). MBP/β-gal double labeling was also detected (Fig. 6D).

The differentiation potential of transplanted cells appeared to depend on the location of cells relative to the injection site. Many nonmigratory cells near the injection site remained as undifferentiated nestin$^+$ cells (Fig. 6B). In contrast, β-gal$^+$ cells that migrated away from the injection site to the contralateral hemisphere expressed astrocytic lineage markers and, when in neurogenic regions, neuronal markers (Fig. 6A, C and Supplementary Fig. 2). When the total number of β-gal$^+$ cells was counted in multiple coronal brain sections, we found that ~12% of the surviving cells adopted a neuronal phenotype (NF/β-gal), while ~17% adopted an astrocyte lineage (GFAP/β-gal), and up to 2% to oligodentrocytes (MBP/β-gal). The remainder persisted as undifferentiated precursor cells. As we previously demonstrated (26), we do not believe the donor cells impart a beneficial effect via neural cell replacement per se, but rather through molecular mechanisms; therefore, the differentiation profile is interesting but not critical. The important findings are that no neoplasms or inappropriate cell types were detected. There was no cell overgrowth or deformation.

DISCUSSION

After transplanting migratory NSCs into a single site in a mouse model of Sandhoff disease during the adult symptomatic phase of this neurodegenerative disorder, a 19% improvement in life expectancy resulted. We previously assessed the efficacy of stem cell therapy on neonatal presymptomatic Sandhoff diseased mice and showed a clinical benefit accompanied by a 40% increase in life expectancy (12). These data suggest that, while early stem cell therapy provides the greatest efficacy, therapy initiated after diagnosis may provide clinical benefit to Sandhoff patients. In neonatal animals, adding a substrate-reducing drug along with NSC transplantation demonstrated synergy by doubling the lifespan in some animals (26). It is possible that adding such pharmacologic therapy to cellular therapy in adult symptomatic animals, could have a similar synergic effect. The present studies also relied on the NSCs' constitutive inherent production of HexB. It may be that engineering the NSCs to overexpress HexB could enhance recovery even further.

Stem cell injection at midsymptomatic (12–13 weeks) stages of disease resulted in progressive migration of stem cells from injection sites to multiple brain regions, including the noninjected contralateral hemisphere. Stem cells delayed disease progression through a combination of cellular and molecular effects, principally donor-to-recipient cross correction via enzyme secretion-recapture, tropic support or anti-inflammatory or immune modulatory effects. Neural cell replacement may have played a minor role. The ability of the normal enzyme to be released from the transplanted cells and "cross-correct" diseased cells – stem cells acting as an enzyme source – appears beneficial even in established disease.

Expression of TNFα, IL1β, MIPα, and Mac1α is elevated in both mouse models of Sandhoff disease and in human patients (2,3). Expression of these inflammatory genes was downregulated following NSC therapy. An inflammatory milieu existing in a chronic disease may generate a gradient of inflammatory or chemotactic molecules, which may act as long-range signals, directing migration of stem cells to sites of pathology. In support of this idea, extensive migratory responses were not observed in the wild-type adult brain. Furthermore, NSCs appeared to be drawn to regions of T2 hyperintensity by MRI, not seen in wild type mice.

The molecular basis for this pathotropism remains unclear and needs to be defined, as modulation of these signals may enhance transplantation benefits. This is particularly relevant to clinical intervention in early presymptomatic disease when signals may be weak.

In chronically diseased brains of juvenile or adult mice, chemotaxis allows cells to mediate beneficial actions at sites distant from the injection site hence allowing the number of injection sites to be minimized. SCF is among the potential chemotactic molecules implicated in pathotropism (27). However, based on RT-PCR results, SCF-mediated NSC migration in this experimental setting was not clear, suggesting that other unidentified factors mediate this activity. However, highly elevated MIP1α (CCL3), which is secreted from reactive astrocytes and damaged neurons(25), may stimulate chemotactic behavior of stem cells. MIP1α induces chemotaxis, adhesion, and cell recruitment by interacting with the G-protein-coupled chemokine receptors CCR1 and CCR5, which are constitutively expressed by NSCs (28). Whether this chemokine causes upregulation of these receptors remains to be determined.

Transplanted NSCs may rectify disease-related host gene expression, although the underlying mechanisms are unclear. We hypothesize that grafted stem cells exert this effect through intrinsic immune modulatory properties. These effects may also occur through reduction of lysosomal storage via metabolic cross correction or a combination of these events. These findings extend observations that BMT and substrate reduction therapy protect Sandhoff mice (19), slowing both inflammation and neurodegeneration. Similarly, neuroglial activation in Niemann-Pick Type C mice is suppressed by intracerebral transplantation of bone marrow-derived mesenchymal stem cells (29)

Although previous studies reported benefits of cell-based therapies in mouse models of lysosomal storage disorders, including MPS VII (16,30,31), Krabbe disease (32), metachromatic leukodystrophy (33,34), Niemann–Pick-A (35) and Sandhoff (12) disease, in the majority of these, NSC transplantation was performed in neonates, with a view to arresting disease progression. In a clinical setting, this would be equivalent to *in utero* diagnosis and commencement of therapy prior to symptom onset in early infancy. However, most patients afflicted with these conditions are not investigated and diagnosed until disease symptoms are clinically evident. In other words, the diagnosis is made relatively late. Therefore, therapies that positively impact the disease process in symptomatic individuals need be identified. It is likely that therapy will be more effective if stem cells are engineered to overexpress the specific enzyme deficient in a given disorder, allowing rapid restoration of significant enzyme levels.

In this study, we focused solely on the forebrain as proof-of-concept. In many storage disorders, disease extends to cerebellum, spinal cord and peripheral areas, which contributes to the disease course and symptoms. Therefore, the most effective treatment for these diseases will likely come from combination therapies that target both CNS and peripheral pathologies. Proof of principle of this concept has previously been demonstrated by combining NSCs and substrate reduction therapy in the SD mouse (12).

It is currently unknown whether intervention in even more advanced disease stages would produce benefits. At later stages, inhibitory molecules may be present (4,36) or the local environment may progressively become too toxic and nonpermissive for stem cell survival or repair. More detailed studies are needed to address this issue. Taken together, our findings may have implications for many CNS diseases in which patients are symptomatic at the time of diagnosis, including Alzheimer's and Parkinson's.

Supplementary Material

Refer to Web version on PubMed Central for supplementary material.

References

1. Wraith JE. Lysosomal disorders. Semin Neonatol. 2002; 7:75–83. [PubMed: 12069540]
2. Wada R, Tifft CJ, Proia RL. Microglial activation precedes acute neurodegeneration in Sandhoff disease and is suppressed by bone marrow transplantation. Proc Natl Acad Sci U S A. 2000; 97:10954–9. [PubMed: 11005868]
3. Myerowitz R, Lawson D, Mizukami H, Mi Y, Tifft CJ, Proia RL. Molecular pathophysiology in Tay-Sachs and Sandhoff diseases as revealed by gene expression profiling. Hum Mol Genet. 2002; 11:1343–50. [PubMed: 12019216]
4. Jeyakumar M, Thomas R, Elliot-Smith E, Smith DA, van der Spoel AC, d'Azzo A, Perry VH, Butters TD, Dwek RA, Platt FM. Central nervous system inflammation is a hallmark of pathogenesis in mouse models of GM1 and GM2 gangliosidosis. Brain. 2003; 126:974–87. [PubMed: 12615653]
5. Sango K, Yamanaka S, Hoffmann A, Okuda Y, Grinberg A, Westphal H, McDonald MP, Crawley JN, Sandhoff K, Suzuki K, et al. Mouse models of Tay-Sachs and Sandhoff diseases differ in neurologic phenotype and ganglioside metabolism. Nat Genet. 1995; 11:170–6. [PubMed: 7550345]
6. Phaneuf D, Wakamatsu N, Huang JQ, Borowski A, Peterson AC, Fortunato SR, Ritter G, Igdoura SA, Morales CR, Benoit G, Akerman BR, Leclerc D, Hanai N, Marth JD, Trasler JM, Gravel RA. Dramatically different phenotypes in mouse models of human Tay-Sachs and Sandhoff diseases. Hum Mol Genet. 1996; 5:1–14. [PubMed: 8789434]
7. Jeyakumar M, Dwek RA, Butters TD, Platt FM. Storage solutions: treating lysosomal disorders of the brain. Nat Rev Neurosci. 2005; 6:713–25. [PubMed: 16049428]
8. Suzuki K, Iseki E, Togo T, Yamaguchi A, Katsuse O, Katsuyama K, Kanzaki S, Shiozaki K, Kawanishi C, Yamashita S, Tanaka Y, Yamanaka S, Hirayasu Y. Neuronal and glial accumulation of alpha- and beta-synucleins in human lipidoses. Acta Neuropathol (Berl). 2007; 114:481–9. [PubMed: 17653558]
9. Suzuki K, Iseki E, Katsuse O, Yamaguchi A, Katsuyama K, Aoki I, Yamanaka S, Kosaka K. Neuronal accumulation of alpha- and beta-synucleins in the brain of a GM2 gangliosidosis mouse model. Neuroreport. 2003; 14:551–4. [PubMed: 12657883]
10. Pluchino S, Zanotti L, Rossi B, Brambilla E, Ottoboni L, Salani G, Martinello M, Cattalini A, Bergami A, Furlan R, Comi G, Constantin G, Martino G. Neurosphere-derived multipotent precursors promote neuroprotection by an immunomodulatory mechanism. Nature. 2005; 436:266–71. [PubMed: 16015332]
11. Ourednik J, Ourednik V, Lynch WP, Schachner M, Snyder EY. Neural stem cells display an inherent mechanism for rescuing dysfunctional neurons. Nat Biotechnol. 2002; 20:1103–10. [PubMed: 12379867]
12. Lee JP, Jeyakumar M, Gonzalez R, Takahashi H, Lee PJ, Baek RC, Clark D, Rose H, Fu G, Clarke J, McKercher S, Meerloo J, Muller FJ, Park KI, Butters TD, Dwek RA, Schwartz P, Tong G, Wenger D, Lipton SA, Seyfried TN, Platt FM, Snyder EY. Stem cells act through multiple mechanisms to benefit mice with neurodegenerative metabolic disease. Nat Med. 2007; 13:439–447. [PubMed: 17351625]
13. Wraith, JE. Lysosomal disorders of the brain. Oxford University Press; Oxford: 2004. Clinical aspects and diagnosis; p. 50-77.

14. Ryder EF, Snyder EY, Cepko CL. Establishment and characterization of multipotent neural cell lines using retrovirus vector-mediated oncogene transfer. J Neurobiol. 1990; 21:356–75. [PubMed: 2307979]
15. Snyder EY, Deitcher DL, Walsh C, Arnold-Aldea S, Hartwieg EA, Cepko CL. Multipotent neural cell lines can engraft and participate in development of mouse cerebellum. Cell. 1992; 68:33–51. [PubMed: 1732063]
16. Snyder EY, Taylor RM, Wolfe JH. Neural progenitor cell engraftment corrects lysosomal storage throughout the MPS VII mouse brain. Nature. 1995; 374:367–70. [PubMed: 7885477]
17. Snyder EY. Immortalized neural stem cells: insights into development; prospects for gene therapy and repair. Proc Assoc Am Physicians. 1995; 107:195–204. [PubMed: 8624853]
18. Rosario CM, Yandava BD, Kosaras B, Zurakowski D, Sidman RL, Snyder EY. Differentiation of engrafted multipotent neural progenitors towards replacement of missing granule neurons in meander tail cerebellum may help determine the locus of mutant gene action. Development. 1997; 124:4213–24. [PubMed: 9334270]
19. Jeyakumar M, Norflus F, Tifft CJ, Cortina-Borja M, Butters TD, Proia RL, Perry VH, Dwek RA, Platt FM. Enhanced survival in Sandhoff disease mice receiving a combination of substrate deprivation therapy and bone marrow transplantation. Blood. 2001; 97:327–329. [PubMed: 11133779]
20. Jeyakumar M, Butters TD, Cortina-Borja M, Proia RL, Perry VH, Dwek RA, Platt FM. Delayed symptom onset and increased life expectancy in Sandhoff disease mice treated with N-butyldeoxynojirimycin. Proc Natl Acad Sci USA. 1999; 96:6388–6393. [PubMed: 10339597]
21. Andersson U, Smith D, Jeyakumar M, Butters TD, Borja MC, Dwek RA, Platt FM. Improved outcome of N-butyldeoxygalactonojirimycin-mediated substrate reduction therapy in a mouse model of Sandhoff disease. Neurobiol Dis. 2004; 16:506–15. [PubMed: 15262262]
22. Jeyakumar M, Smith DA, Williams IM, Cortina-Borja M, Neville DCA, Butters TD, Dwek RA, Platt FM. Anti-inflammatory and anti-oxidant therapies increase survival in the Sandhoff disease mouse; synergy with N-butyldeoxynojirimycin. Annals of Neurology. 2004 in press.
23. Hoehn M, Kustermann E, Blunk J, Wiedermann D, Trapp T, Wecker S, Focking M, Arnold H, Hescheler J, Fleischmann BK, Schwindt W, Buhrle C. Monitoring of implanted stem cell migration in vivo: a highly resolved in vivo magnetic resonance imaging investigation of experimental stroke in rat. Proc Natl Acad Sci U S A. 2002; 99:16267–72. [PubMed: 12444255]
24. Neville DC, Coquard V, Priestman DA, te Vruchte DJ, Sillence DJ, Dwek RA, Platt FM, Butters TD. Analysis of fluorescently labeled glycosphingolipid-derived oligosaccharides following ceramide glycanase digestion and anthranilic acid labeling. Anal Biochem. 2004; 331:275–82. [PubMed: 15265733]
25. Zhang SC, Fedoroff S. Expression of stem cell factor and c-kit receptor in neural cells after brain injury. Acta Neuropathol (Berl). 1999; 97:393–8. [PubMed: 10208279]
26. Lee JP, Jeyakumar M, Gonzalez R, Takahashi H, Lee PJ, Baek RC, Clark D, Rose H, Fu G, Clarke J, McKercher S, Meerloo J, Muller FJ, Park KI, Butters TD, Dwek RA, Schwartz P, Tong G, Wenger D, Lipton SA, Seyfried TN, Platt FM, Snyder EY. Stem cells act through multiple mechanisms to benefit mice with neurodegenerative metabolic disease. Nat Med. 2007; 13:439–47. [PubMed: 17351625]
27. Sun L, Lee J, Fine HA. Neuronally expressed stem cell factor induces neural stem cell migration to areas of brain injury. J Clin Invest. 2004; 113:1364–74. [PubMed: 15124028]
28. Martino G, Pluchino S. The therapeutic potential of neural stem cells. Nat Rev Neurosci. 2006; 7:395–406. [PubMed: 16760919]
29. Bae JS, Furuya S, Ahn SJ, Yi SJ, Hirabayashi Y, Jin HK. Neuroglial activation in Niemann-Pick Type C mice is suppressed by intracerebral transplantation of bone marrow-derived mesenchymal stem cells. Neurosci Lett. 2005; 381:234–6. [PubMed: 15896475]
30. Meng XL, Shen JS, Ohashi T, Maeda H, Kim SU, Eto Y. Brain transplantation of genetically engineered human neural stem cells globally corrects brain lesions in the mucopolysaccharidosis type VII mouse. J Neurosci Res. 2003; 74:266–77. [PubMed: 14515356]

31. Karolewski BA, Wolfe JH. Genetic correction of the fetal brain increases the lifespan of mice with the severe multisystemic disease mucopolysaccharidosis type VII. Mol Ther. 2006; 14:14–24. [PubMed: 16624622]

32. Taylor RM, Lee JP, Palacino JJ, Bower KA, Li J, Vanier MT, Wenger DA, Sidman RL, Snyder EY. Intrinsic resistance of neural stem cells to toxic metabolites may make them well suited for cell non-autonomous disorders: evidence from a mouse model of Krabbe leukodystrophy. J Neurochem. 2006; 97:1585–99. [PubMed: 16805770]

33. Klein D, Schmandt T, Muth-Kohne E, Perez-Bouza A, Segschneider M, Gieselmann V, Brustle O. Embryonic stem cell-based reduction of central nervous system sulfatide storage in an animal model of metachromatic leukodystrophy. Gene Ther. 2006

34. Pellegatta S, Tunici P, Poliani PL, Dolcetta D, Cajola L, Colombelli C, Ciusani E, Di Donato S, Finocchiaro G. The therapeutic potential of neural stem/progenitor cells in murine globoid cell leukodystrophy is conditioned by macrophage/microglia activation. Neurobiol Dis. 2006; 21:314–23. [PubMed: 16199167]

35. Shihabuddin LS, Numan S, Huff MR, Dodge JC, Clarke J, Macauley SL, Yang W, Taksir TV, Parsons G, Passini MA, Gage FH, Stewart GR. Intracerebral transplantation of adult mouse neural progenitor cells into the Niemann-Pick-A mouse leads to a marked decrease in lysosomal storage pathology. J Neurosci. 2004; 24:10642–51. [PubMed: 15564580]

36. Proia RL, Wu YP. Blood to brain to the rescue. J Clin Invest. 2004; 113:1108–10. [PubMed: 15085187]

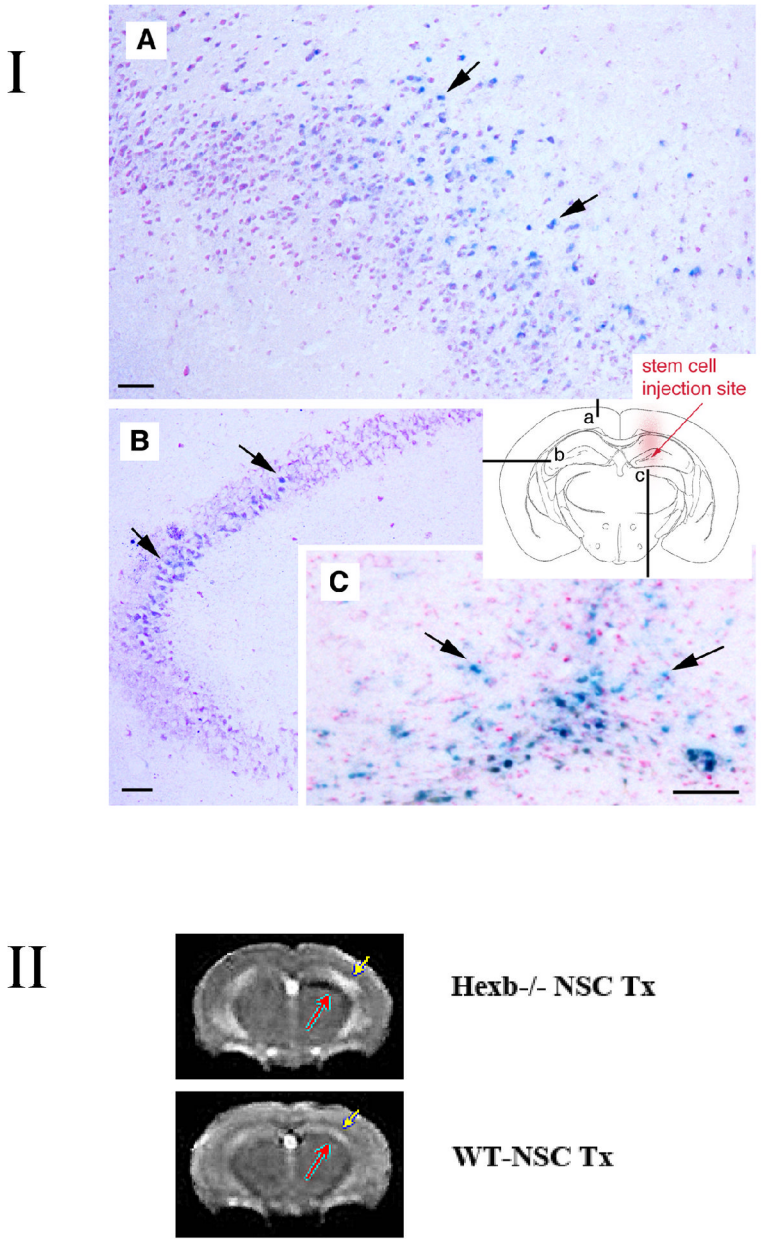

Figure 1.

I. **NSC transplants survive and engraft in Sandhoff disease *Hexb*$^{-/-}$ mouse model.** Adult symptomatic mice 12–13 weeks of age were used. Using a stereotaxic frame (KOPF®), through a 0.9-mm diameter hole in the skull (2-mm posterior to bregma; 1.5-mm lateral to sagittal suture), 4 μl (8×10^4 cells/μl) of C17.2 cells in PBS was injected unilaterally into the hippocampus (right hemisphere) under isofluorane anaesthesia. Mock-grafted controls received the same volume of PBS. Coronal brain sections were permeabilized with detergents and exposed to a chromogenic substrate X-gal to detect β-gal-labeled donor cells. The blue cells (X-gal histochemical reaction, arrows) have engrafted in the recipient brain with widespread migration, distribution, and integration. Representative images of the brain (A–C) from 15-week-old *Hexb*$^{-/-}$ mice are shown (n=7). Schematic

diagram (a–c) illustrates where images are from (images A–C, respectively) in relation to injection site. Scale bar = 10 μm. Counter stain = neutral red.

II. Noninvasive MRI tracking of neural stem cells in live mice. T2-weighted image acquired with a fast spin-echo sequence (TR=3s, TE=48ms), 1-mm coronal slice with an in-plane resolution of 234 μm, at posttransplantation day 38. Injection site of Sinerem®-labeled stem cells is clearly visible (red arrow) in the right hemisphere of *Hexb*$^{-/-}$ mice, while minimal change in signal intensity is evident in the wild-type transplanted mice which had received the same number of Sinerem®-labeled stem cells. More NSCs (black, red arrow) are located juxtaposed to T2 hyperintensity in the cortex (yellow arrow, which could represent increased inflammation) compared to similarly transplanted NSCs in wild type mice, which show no such T2 signal (yellow arrow) & very few, if any, NSCs (black, red arrow) accumulating in the cortex). Although the main migration streams were detected with MR, the technique does not have the sensitivity to detect lower cell densities readily detected histologically. n=2 per group.

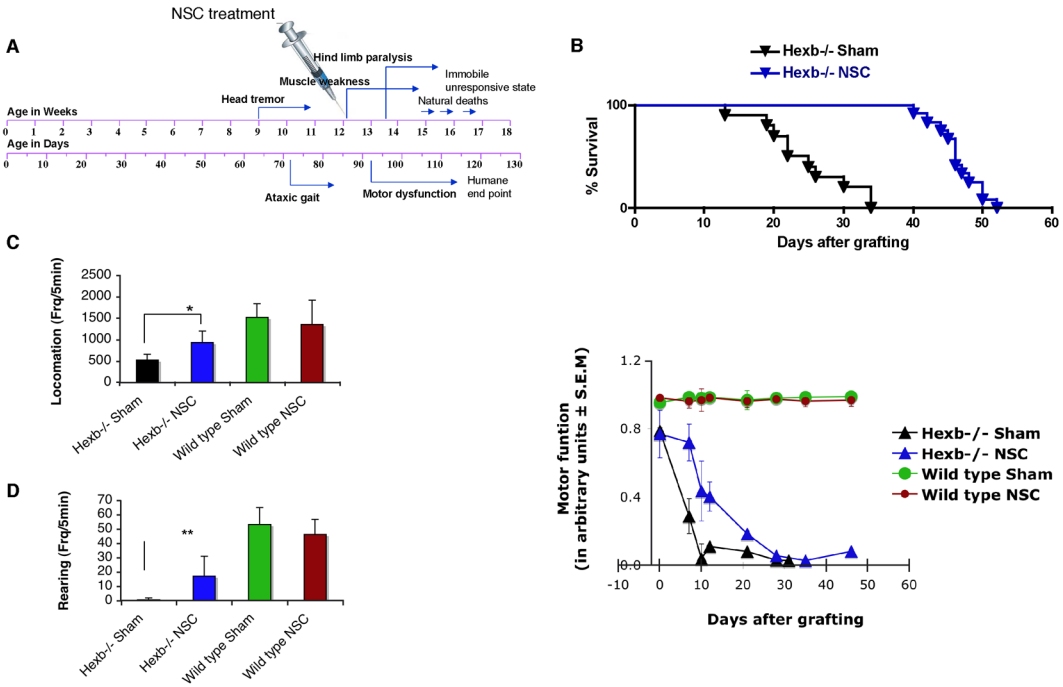

Figure 2. NSC transplants improve lifespan and delay rate of disease progression in symptomatic adult *Hexb*$^{-/-}$ mice

NSCs, not engineered to overexpress HexB, were injected into one site of non-immunosuppressed adult SD mice. (A) Schematic of symptom onset and kinetics of disease progression in Sandhoff disease (*Hexb*$^{-/-}$) mice. (B) Survival of NSC-transplanted mice (n=12) compared with sham-treated control *Hexb*$^{-/-}$ mice (n=10). NSC transplantation prolonged *Hexb*$^{-/-}$ mice lifespan by 21 days ($p<0.0001$, Log rank test), resulting in a 19% improvement in survival. (C, D) Neurologic function scored in an automated activity monitor, which records infrared beam breaks in the X -Y plane (locomotion) and vertical (rearing) movements (data at 2 weeks posttreatment, 15 weeks of age). Data represent mean ± s.e.m, n=6 per group. An unpaired two-tailed Student's t-test was used to compare data for significance. (E) Temporal profile of motor function before and after NSC treatment. Motor function was assessed using a horizontal bar-crossing test measuring the latency to cross or fall from the bar. Motor-function decline was significantly delayed in the NSC-treated SD mice, compared to the sham-treated SD control group ($p<0.0001$, two-way ANOVA). Data represent mean ± s.e.m, n=7–12.

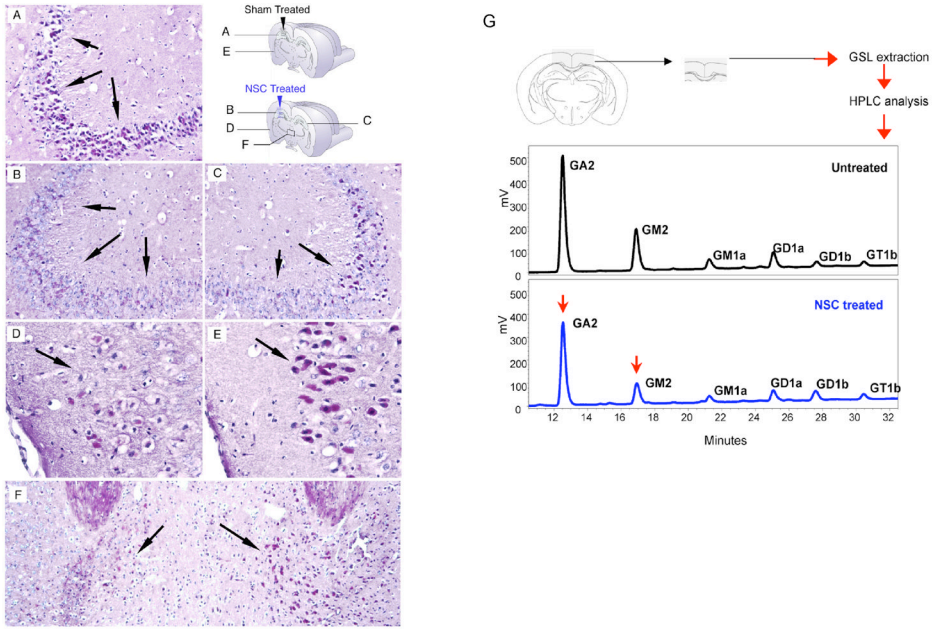

Figure 3. Reduction of GSL storage in brains of NSC-treated *Hexb*$^{-/-}$ mice

(A–F) Representative PAS staining from brain sections of NSC-treated and sham-treated control mice at 15 weeks of age (n=4 per group). Storage GSLs were visualised in frozen brain sections by PAS staining (red). Panels A and E show sham-injected hemisphere of control *Hexb*$^{-/-}$ mice; panels B and D represent injected hemisphere of NSC-treated *Hexb*$^{-/-}$ mice; panel C represents noninjected hemisphere of NSC-treated *Hexb*$^{-/-}$ mice; panel F represents a region of thalamus of NSC-treated *Hexb*$^{-/-}$ mice. Hippocampus CA3 region (A–C), mediodorsal thalamic nucleus (F), and late entrohinal cortex (D, F) are shown. By 3 weeks posttransplant, the hippocampus of NSC-treated *Hexb*$^{-/-}$ mice showed less PAS-positive GSL storage (B and C, compared with A), the most significant reduction achieved in the injected hemisphere, compared to the noninjected hemisphere in the same animal (C compared with B). (G) Representative HPLC profile of cerebral cortical region of NSC-treated and sham-treated *Hexb*$^{-/-}$ mice are shown 2 weeks posttreatment (n=4 per group). GM2 was reduced by 19±1% (p=0.004) while GA2 was reduced by 8±0.3% (p=0.015) in the brain region shown, as analyzed by HPLC. An unpaired two-tailed Student's t-test was used to compare data for significance.

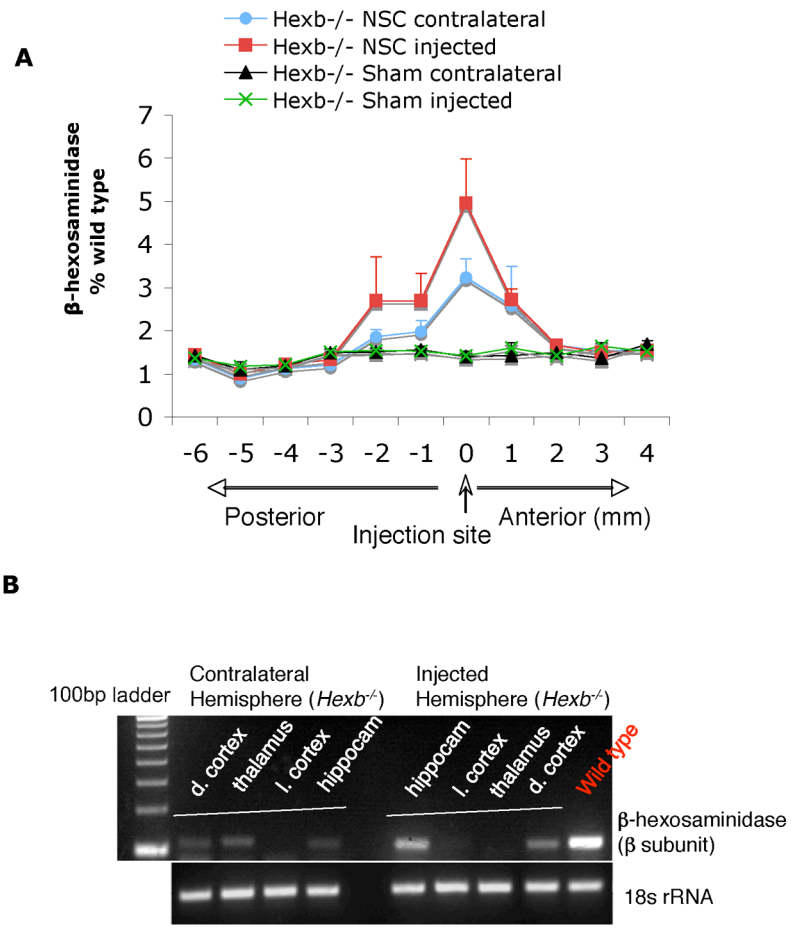

Figure 4. Increased β-hexosaminidase enzyme levels in brains of NSC-treated *Hexb*$^{-/-}$ mice

(A) Representative Hex levels in serial coronal brain sections of individual hemisphere from NSC-treated and sham-treated *Hexb*$^{-/-}$ mice at 4 weeks posttransplant. Brain homogenates were made from 12 individual brain slices, as per schematic diagram, and hex levels were measured against 4-MUGlcNAc artificial substrate (mean ± s.e.m., n=3). Ipsilateral represents the injected hemisphere, while contralateral represents the noninjected hemisphere. (B) RT-PCR analysis for β-subunit expression of Hex from local brain regions. Two or more brain regions (dorsal cortex/thalamus/lateral cortex/hippocampus) expressed the Hexβ-subunit gene in each hemisphere, indicative of donor-derived cell migration and brain engraftment upon unilateral (hippocampus) NSC transplantation.

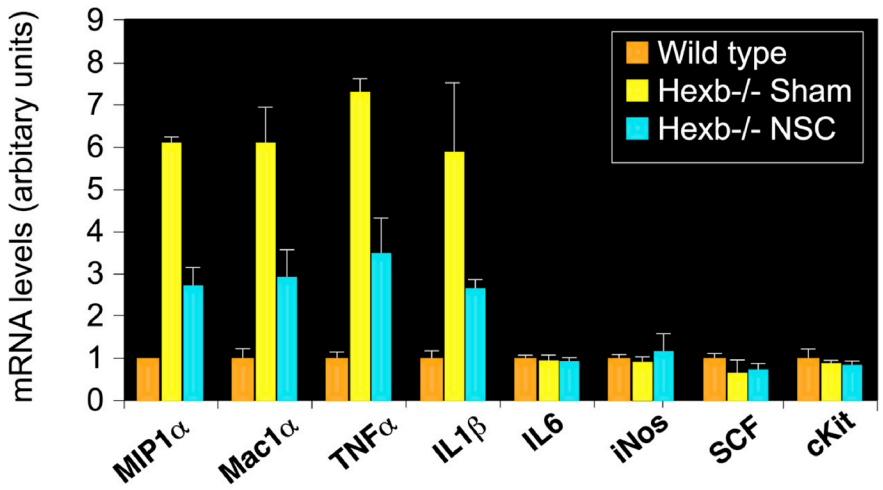

Figure 5. Reduced inflammatory marker expression in brains of NSC-treated *Hexb*$^{-/-}$ mice

Expression of inflammatory genes in mouse brains as measured by RT-PCR. The relative gene expression normalized with 18S RNA (arbitrary units) is shown on the graphs. Accompanied by increased levels of microglial/macrophage activation marker Mac1α (Cd11b) ($p<0.001$), proinflammatory cytokines TNFα and IL-1β and the chemokine MIP1α (CCL3), expression levels were high in the diseased mice, compared to the wild-type mice ($p<0.001$). Upon NSC treatment, all upregulated genes were reduced significantly when the age-matched sham-treated control group was compared ($p<0.001$). No significant changes in IL-6, iNOS, SCF or c-kit expression were observed. Data are mean ± s.e.m. based on 3–5 animals in each group (R and L hemispheres averaged together). An unpaired two-tailed Student's t-test was used to compare data for significance.

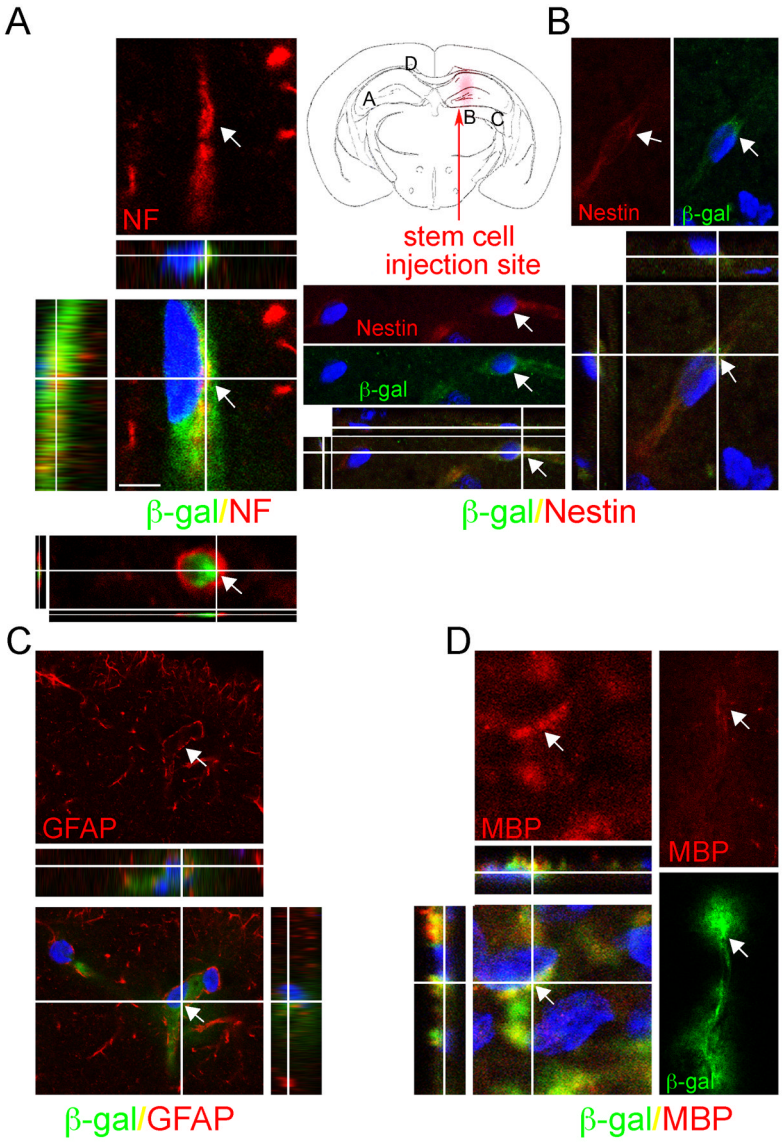

Figure 6. Engrafted NSCs differentiate into a range of neural cell types in the *Hexb*$^{-/-}$ mouse brain

Following NSC transplantation at 13 weeks of age, brains of *Hexb*$^{-/-}$ mice were processed for cell type characterization using immunoflourescence staining for both LacZ expressed β-gal and neural cell-type specific markers. At 3 weeks posttransplant, NSCs stably engrafted in the *Hexb*$^{-/-}$ mouse brain, differentiating into a range of neural cell types. (A–D) Representative donor-derived cells, recognized by their immunoreactivity to β-gal (green, bottom), coexpress neuronal markers such as neurofilament (NF), astroglial marker GFAP, oligodentrocyte marker MBP and nestin, a marker of undifferentiated neural precursors. Merged images show blue DAPI nuclear staining identifies all cells in the field (bottom). Each merged image is also shown as an orthogonal projection composed of 9–16 optical Z-planes, 0.5–1 μm thick. Arrows in each panel of a given column indicate the same cell. Scale bar = 10 μm. (see also Supplementary Fig 2).